

Analytical Model for E-Shaped Microstrip Patch Antenna

Kim H. Yeap¹, Widad Ismail¹, and Kim H. Yeap²

¹ School of Electrical and Electronic Engineering
Universiti Sains Malaysia, Engineering Campus, Seberang Perai Selatan, 14300 Nibong Tebal, Penang, Malaysia
kimhuat18@gmail.com, eewidad@usm.my

² Department of Electronic Engineering
Universiti Tunku Abdul Rahman, Jalan Universiti, Bandar Barat, 31900 Kampar, Perak, Malaysia
yeapkh@utar.edu.my

Abstract — This paper presents a comprehensive insight of the E-shaped microstrip patch antenna through the introduction of its cavity model and circuit model. The cavity model of the E-shaped antenna postulates a central magnetic wall that subdivides the structure into two halves, each with the TM_{001} field configuration. On the other hand, the circuit model is formulated based on the segmentation yielded from the cavity model. It infers the dual-resonance of the antenna through its circuit equivalent aspect, while avoiding cumbersome computations. Both these models offer an in depth view on the operating principles of the E-shaped antenna and effectively relates to its desired performance. A proof-of-concept design has been implemented. With the size of $147 \times 112 \text{ mm}^2$, the antenna design resonates at 2.4 GHz and 2.5 GHz. It is noted that the reflection coefficients of its circuit model yield a deviation of less than 4 dB from the actual board measurement.

Index Terms — Cavity model, circuit equivalent, current distribution, E-shaped, microstrip antenna.

I. INTRODUCTION

Communication technology today serves to improve the efficiency of not only industrial systems, but also various services like military applications and medical area [1]. One of the popular patch antennas design used in the communication technology is the E-shaped microstrip patch antenna. Resembling the letter “E” in appearance, this antenna exhibits a dual-resonant behaviour on a single radiating structure, thus produces two different frequencies concurrently. Such feature avoids the need of separate antennas and provides antenna size reduction. Its applications include vehicular-satellite communication modules as well as synthetic-aperture radars (SAR) and multi-spectral scatterometers. Its potential is deemed promising.

Throughout the years, numerous research works have been performed on the E-shaped antenna [2-11],

mostly conducted with computer-aided design (CAD) simulations, as summarized in Table 1. The utilization of CAD tools, such as HFSS and CST, is apparently indispensable. However it is equally important for not to solely rely on the tool itself but also to appreciate its operational insight, as exemplified in [12]. This is well evident in the case of the rectangular patch, where the introduction of its transmission line model and cavity model has since played a revolutionary role that realizes patch designs of miscellaneous sizes and geometries.

To date, the available literature on a detailed elaboration of the E-shaped patch design appears yet to require a rigorous treatment of the topic, not to mention its operating principle and design computation [7-11]. This is much due to its arbitrary shape and complex structure.

Table 1: Summary for researches on E-shaped antenna

Work	Frequency (GHz)	Simulation Tool	Features
[2]	1.9, 2.4	HFSS	30.3% bandwidth
[3]	2.4	HFSS	Suitable for MIMO applications
[4]	5.05 – 5.88	HFSS	Trim length of centre arm to tune resonances
[5]	1.9 – 2.4	IE3D	32.5% bandwidth
[6]	12, 14.5	CST	Add six slits and a trapezoidal slot to tune resonances
[7]	5 – 6	HFSS	Suitable for WLAN adaptor cards
[8]	0.75 – 0.97	IE3D	Reduces 50% antenna size with tapered slots
[9]	4.5 – 8.5	IE3D	57.36% bandwidth
[10]	5 – 6	Ensemble, HFSS	20% bandwidth
[11]	3.05 – 11.8	HFSS	Achieves ultra wideband using triple E-shaped structures

As the dual-resonance of the E-shaped antenna requires similar radiation patterns and impedance matching, the study on its basic characteristics and resonance model is critical. This study offers an in depth view of its inherent mechanism and opens a path for not only resolving its parametric issues but also anticipating future optimizations. It is attributed to this prominent reason that this paper offers a comprehensive yet concise explication on the operation of the E-shaped antenna through the introduction of its cavity model and circuit equivalent model.

II. CURRENT DISTRIBUTION AND SEGMENTATIONS

The intrinsic mechanism of the E-shaped patch antenna is intimately associated to its current distribution as shown in Fig. 1. It appears that the E-shape is forged from a rectangular patch by inseting a pair of parallel slots into it. The slots contribute to the current perturbations on the patch structure. As a result, the current flowing in the centre and at the side crosses over each other by meandering along the slots. It is also observed that the surface current concentrates on the centre and scatters at both sides. When scrutinized, the intense current flow along the central path actually forms a mirror line, breaking the antenna into two symmetrized halves. Details on this shall be elaborated in Section III.

Figure 2 illustrates a typical E-shaped patch antenna that is segmented into four sections, namely the dominant section ($S_{dominant}$), the centre section (S_{centre}), and two side sections (S_{side} 's). In principle, however, it is less legitimate to segment the antenna with a definite boundary, since the geometries of each patch are structurally inter-related. The segmentation here, nonetheless, is intended to facilitate its analysis.

$S_{dominant}$ plays the major part in the design, which is responsible for the overall radiation behaviour of the antenna. It determines the antenna resonance range and field configuration. $W_{dominant}$ and $l_{dominant}$ denotes the respective width and length of $S_{dominant}$, while h is the height of the patch substrate. S_{side} and S_{centre} fine-tune $S_{dominant}$ to resonate at the desired frequency precisely. W_{side} and l_{side} denotes the respective width and length of S_{side} , while W_{centre} and l_{centre} denotes the respective width and length of S_{centre} . $\hat{\tau}$ and \hat{n} are the tangential and normal components, respectively.

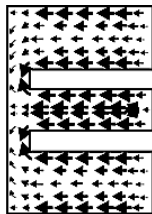


Fig. 1. Current distribution of E-shaped antenna [13].

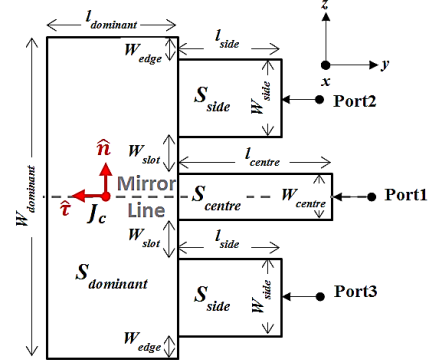


Fig. 2. Segmentation of E-shaped antenna.

III. METHODS OF ANALYSIS

The inherent principle of an E-shaped antenna is operationally complex. By studying its operating mechanism, the cavity model and circuit model have been developed to provide a methodological platform in gaining a deeper insight of its pragmatic nature while in perseverance of its simplicity.

A. Cavity model for E-shaped antenna

It is known a priori that the cavity model for a rectangular patch antenna, the region between the patch and its ground plane is conceived as an electromagnetic (EM) cavity that is bounded by magnetic walls around the periphery and by electric walls on the top and bottom sides [14]. When the patch is energized, the attractive tendency concentrates the charges on the bottom surface while the repulsive tendency pushes the like charges on the bottom surface along the edge to the top. This creates the current densities J_t and J_b on its respective top and bottom surface.

For very thin substrate ($h \ll \lambda$), the attractive tendency dominates and most of the charges concentrate on the bottom of the patch. The current flows along the edges are very small and ultimately assumed zero. Consequently, the tangential component of the magnetic field (H_τ) along the edge is assumed zero as well. Hence, the side walls are modelled as perfect magnetic conductors. Assuming that the patch is perfectly conductive, the electric field bounded by the magnetic walls renders no tangential component (E_τ) in the normal direction. As such, the electric field is only normal directed to the patch while the magnetic field has only the transverse components in the region bounded by the patch metallization and ground plane. This creates the electric walls on the top and bottom of the cavity. According to [15], by the equivalence principle, the current densities along the periphery of the cavity are found as:

$$\mathbf{J}_s = \hat{n} \times \mathbf{H}_a \text{ and } \mathbf{M}_s = -\hat{n} \times \mathbf{E}_a. \quad (1)$$

It is noted that this formulation is exact but requires integration over its closed surface. \mathbf{J}_s , \mathbf{M}_s is the

respective electric and magnetic current density while \mathbf{E}_a , \mathbf{H}_a is the respective electric and magnetic field. \mathbf{J}_s , \mathbf{J}_t are zero due to the thin substrate assumption and from image theory,

$$\mathbf{M}_s = -2\hat{n} \times \mathbf{E}_a, \quad (2)$$

resulted by the presence of the ground plane.

Due to the arbitrary shape of the patch, $S_{dominant}$ is analyzed as it governs the overall field configuration. With $W_{dominant} > \frac{W_{dominant}}{2} > l_{dominant} > h$, $S_{dominant}$ operates in the TM_{002} mode and its cavity model is shown in Fig. 3 (a). With the horizontal mirror line observed from its current distribution and referring to Fig. 2, the surface current density along the line (\mathbf{J}_c) can be dissolved as:

$$\mathbf{J}_c = \hat{t} \cdot \mathbf{J}_c + \hat{n} \cdot \mathbf{J}_c = -\hat{y} \cdot \mathbf{J}_c + \hat{z} \cdot \mathbf{J}_c, \quad (3a)$$

since \hat{t} is proportional to the reverse \hat{y} direction while \hat{n} is proportional to the \hat{z} direction. From Fig. 1, \mathbf{J}_c is purely tangential, therefore,

$$\mathbf{J}_c = -\hat{y} \cdot \mathbf{J}_c. \quad (3b)$$

Similar to the derivation for \mathbf{J}_s in (1),

$$\mathbf{J}_c = \hat{x} \times \mathbf{H}, \quad (4)$$

where \mathbf{H} is the magnetic field on the patch. Applying $(-\hat{x} \times)$ to both sides and substituting (3b) into (4),

$$\mathbf{H} = -\hat{x} \times (-\hat{y} \cdot \mathbf{J}_c) = \hat{z} \cdot \mathbf{J}_c = \hat{n} \cdot \mathbf{J}_c. \quad (5)$$

The resultant \mathbf{H} coincides with that at its periphery, where \mathbf{H} has only a normal component along the mirror line of the patch. The zero tangential \mathbf{H} component implies that a magnetic wall is formed along its centre. Consequently, $S_{dominant}$ is subdivided into two symmetrical halves, $S'_{dominant}$ with each width, $W'_{dominant}$ being:

$$W_{dominant} = 2W'_{dominant}. \quad (6)$$

Likewise, S_{centre} is split into two mirrored halves, S'_{centre} 's and each with width, W'_{centre} . Hence,

$$W_{centre} = 2W'_{centre}. \quad (7)$$

With $W'_{dominant} > l_{dominant} > h$ for $S'_{dominant}$, its field configuration is TM_{001} and reflects a mirrored complement as shown in Fig. 3 (b). One crucial emphasis is \mathbf{M}_s found with (1). Its opposite flow on the central magnetic wall notably signifies a counter effect, thereby cancelling its radiation at the centre of the patch. Correspondingly, the field propagating along the magnetic wall at both its edges with length, $l_{dominant}$ forms a pair of radiating slots on the antenna.

From the analysis of its current distribution and with reference to its dimensions, the electric field (E) and magnetic (H) components are expressed as [16]:

$$E_x = -j\omega A_{002} \cos\left(\frac{2\pi}{W_{dominant}} z'\right), \quad (8)$$

$$H_y = -\frac{2\pi}{\mu W_{dominant}} A_{002} \sin\left(\frac{2\pi}{W_{dominant}} z'\right), \quad (9)$$

$$E_y = E_z = H_x = H_z = 0, \quad (10)$$

where the subscripts x , y , z for E and H denote its respective x , y , z direction. A_{002} represents the amplitude coefficient of the TM_{002} mode while z' represents the

field within the cavity. In conjunction with E and H as well as by associating it with the width of a basic rectangular patch (W) [15], the resonant frequency of the antenna (f_r) at its dominant mode is expressed as:

$$(f_r)_{002} = \frac{v_0}{W_{dominant}} \sqrt{\frac{2}{\epsilon_r + 1}}. \quad (11)$$

B. Circuit model for E-shaped antenna

While the cavity model interprets the patch antenna from its charge distribution perspective, the circuit model infers its return losses (RLs) in circuitual analogy. Its conception is purely schematic, where the mechanism of the overall patch is manifested with the elements of a high-frequency circuit network.

It has been broadly documented that the E-shaped patch antenna could be analogically represented by two inductor-capacitor (LC) resonant tanks [3], as portrayed in Fig. 4. Its first resonance is exhibited by the original rectangular patch while its second resonance is caused by the slots then inserted. Along the centre of the patch, the current flows like the rectangular design [17], where the inductance, L_r is attributed to the current path length while the capacitance, C_r is subjected to the sandwich-like structure of the substrate bounded by the patch and ground layers. At the sides of the patch, its current circumnavigates across the slots, causing an increase in its current path. The effect is modeled as an additional series inductance, ΔL_r while the slot between the centre and side of the patch yields an additional parallel capacitance, ΔC_r . As a result, the sides of the patch resonate at a lower frequency [18].

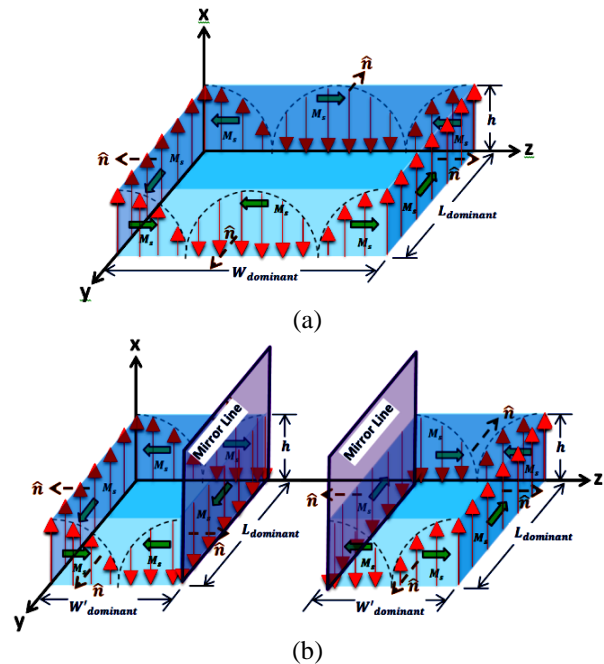


Fig. 3. (a) TM_{002} and (b) mirrored halves of $S_{dominant}$.

The LC representation is by no mean the exact model of the E-shaped patch, but merely presents a theoretical explanation of its dual-resonance principle. In [2, 3] for instance, two LC shunt tanks are presented while in [4], two LC series tanks are shown instead. In a much entirely manner, [5, 6] analyze the E-shaped patch design by introducing a full circuit model. The models are introduced in the form of a resistor-inductor-capacitor (RLC) network, which take into account the inherent losses of the patch. Its analysis are elaborated in detail and supported with formulations. Nevertheless, the models are portrayed on a conceptual basis, and lack of prognostication of the antenna characteristics. Conversely, the antennas reported in [7-11] are designed with the aid of CAD tools.

Contrast to the previous models, the circuit equivalent model in this paper presents a full and comprehensive view of the E-shaped patch along with straightforward circuit formulations. In addition, the proposed circuit network is also able to emulate the performance of the actual design, such as its impedance bandwidth and RL. The synthesis of the LC circuit principle with the segmentation from the cavity model brings forth the formation of the proposed circuit network in Fig. 5. In this model, $S'_{dominant}$ adopts the transmission line model of a rectangular patch and is visualized as two radiating slots separated by a transmission line [15]. Its electric field propagation is nonhomogeneous, whereby the major part concentrates in the substrate and the remaining part resides in open space. Hence, an effective dielectric constant, ϵ_{reff} is introduced to account for the fringing effects,

$$\epsilon_{reff} = \frac{\epsilon_r + 1}{2} + \frac{\epsilon_r - 1}{2} \left[1 + 12 \frac{h}{W} \right]^{-\frac{1}{2}}, \quad \frac{W}{h} > 1, \quad (12)$$

where ϵ_r is the dielectric constant. The fringing length, Δl and length, l of the patch are respectively given as:

$$\Delta l = 0.412h \frac{(\epsilon_r + 0.3) \left(\frac{W}{h} + 0.264 \right)}{(\epsilon_r - 0.258) \left(\frac{W}{h} + 0.8 \right)}, \quad (13)$$

$$l = \frac{v_o}{2f_r \sqrt{\epsilon_{reff}}} + 2\Delta l, \quad (14)$$

where v_o is the speed of light in free space.

The two radiating slots are represented by two identical lines of equivalent admittance, Y_1 and Y_2 as:

$$Y_1 = Y_2 = G_1 + jB_1, \quad (15)$$

$$G_1 = G_2 = \frac{d}{120\lambda_o} \left[1 - \frac{1}{24} (k_o h)^2 \right], \quad \frac{h}{\lambda_o} < \frac{1}{10}, \quad (15a)$$

$$B_1 = B_2 = \frac{d}{120\lambda_o} \left[1 - 0.636 \ln(k_o h) \right], \quad \frac{h}{\lambda_o} > \frac{1}{10}, \quad (15b)$$

where λ_o and k_o is the respective wavelength and wavenumber in free space, G is the conductance and B is the susceptance of the radiating slot. d denotes the length of the slot, that is $l_{dominant}$ for $S'_{dominant}$. Both radiating slots are shorted by a high-admittance transmission line. Thus, its radiation resistance, $R_{dominant}$ and capacitance, $C_{dominant}$ are found by:

$$R_{dominant} = \frac{1}{G_1} = \frac{1}{G_2}, \quad (16)$$

$$C_{dominant} = \frac{B_1}{2\pi f_{dominant}} = \frac{B_2}{2\pi f_{dominant}}, \quad (17)$$

where $f_{dominant}$ is the resonant frequency for $S'_{dominant}$. The conductive and dielectric losses are deemed negligible due to its very thin metallization and substrate layers in comparison with the overall dimension of $S'_{dominant}$.

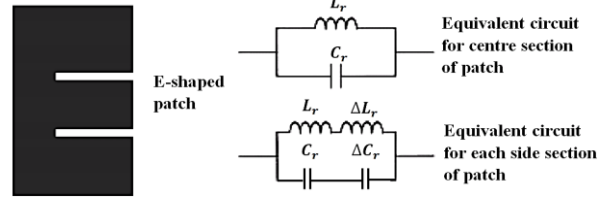


Fig. 4. LC representation of E-shaped antenna.

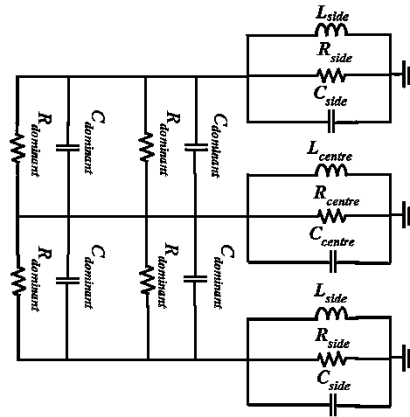


Fig. 5. Circuit equivalent model of E-shaped antenna.

In association to the LC resonant effect, S_{side} and S_{centre} are each modelled as a parallel RLC network. The total resonant resistance, R_{res} accounts for both the radiation resistance, R_r [19] and dielectric loss, R_d [20] while the conductive loss is comparatively negligible.

$$R_{res} = R_r + R_d, \quad (18)$$

$$R_d = \frac{30 \tan \delta h \lambda_o}{\epsilon_r l W} Q_r^2, \quad (18a)$$

$$R_r = \frac{Q_r}{2\pi f_r C_{res}}, \quad (18b)$$

where $\tan \delta$ is the dielectric loss tangent. Q_r is the radiation quality factor [21] and C_{res} is the capacitance at resonance, which are both given by:

$$Q_r = \frac{v_o \sqrt{\epsilon_{reff}}}{4hf_r} - \frac{\epsilon_{reff} \Delta l}{h}, \quad (19)$$

$$C_{res} = \frac{\epsilon_{reff} \epsilon_o W l}{2h} \cos^{-2} \left(\frac{\pi x_o}{l} \right), \quad (20)$$

where ϵ_o is the permittivity in free space and x_o is the distance of the feed point from the edge of $S'_{dominant}$. The resonant inductance, L_{res} is subsequently found as:

$$L_{res} = \frac{1}{(2\pi f_r)^2 C_{res}}. \quad (21)$$

In (14) – (17), l , W , f_r , and ϵ_{reff} correspond to the respective segment of concern, S_{side} and S_{centre} .

$R_{res} = R_{centre}$, $C_{res} = C_{centre}$, and $L_{res} = L_{centre}$ with regards to S_{centre} at resonance, where C_{centre} and L_{centre} are respectively denoted by C_r and L_r in the LC circuit representation. Similarly, $R_{res} = R_{side}$, $C_{res} = C_{side}$, and $L_{res} = L_{side}$ with regards to S_{side} at resonance. C_{side} accounts for both C_r and ΔC_r , while L_{side} accounts for both L_r and ΔL_r in the LC circuit representation.

IV. PROPOSED E-SHAPED ANTENNA

In corroborating the conception presented, an E-shaped patch antenna is proposed to operate in the Industrial, Scientific, and Medical (ISM) band. The patch is designed to resonate at 2.5 GHz through S_{centre} and 2.4 GHz through both S_{side} 's. With reference to the designation in Fig. 2, $f_{r_centre} = 2.5$ GHz is excited from Port 1, while $f_{r_side} = 2.4$ GHz is excited from Port 2 and 3, respectively. The antenna is designed on a flame retardant level-4 (FR-4) substrate with $\epsilon_r = 4.5$, $\tan\delta = 0.021$, and $h = 1.6$ mm. Its dimensions are listed in Table 2.

Table 2: Dimensions of proposed E-shaped antenna

Segment	Dimension	Length
$S_{dominant}$	$W_{dominant}$	83.0 mm
	$l_{dominant}$	34.0 mm
S_{centre}	W_{centre}	12.0 mm
	l_{centre}	40.0 mm
S_{side}	W_{side}	20.0 mm
	l_{side}	27.0 mm
Slots	W_{slot}	8.5 mm
	l_{slot}	7.0 mm

A. ADS Momentum design

The proposed antenna is designed using ADS Momentum and the simulated current distribution in Fig. 6 (a) significantly indicates a tangential flow along its centre resembling that in Fig. 1. This substantiated the postulation of a mirror line bisecting the patch into two mirrored halves. Figure 6 (b) visualizes the antenna radiation pattern, which portrays a broadside radiation as customary for microstrip patch antennas.

The simulated co and cross polarizations of its radiation patterns are shown in Fig. 7. Notably, at both resonances, the radiation patterns are rather similar. At the E plane, the peak cross polarization is around 20 dB lower than the peak co polarization while its 3-dB beamwidth is 60°. At the H plane, the peak cross polarization is about 15 dB lower than the peak co polarization while its 3-dB beamwidth is 48°.

Apart from this, a parametric study has been conducted by varying the width of the slot (W_{slot}) from 6.5 mm to 10.5 mm [16], as the slots impose a direct perturbation to the surface current of the patch. The bandwidth response with respect to the changes in W_{slot}

is shown in Fig. 8. It is noted that as W_{slot} expands, the bandwidths at all three ports increase proportionally.

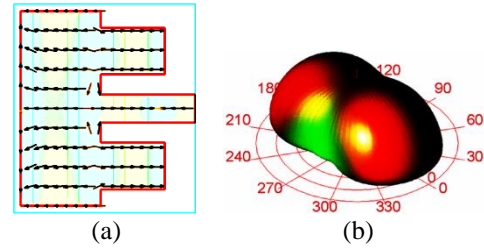


Fig. 6. Simulated (a) current distribution and (b) radiation pattern for proposed E-shaped antenna.

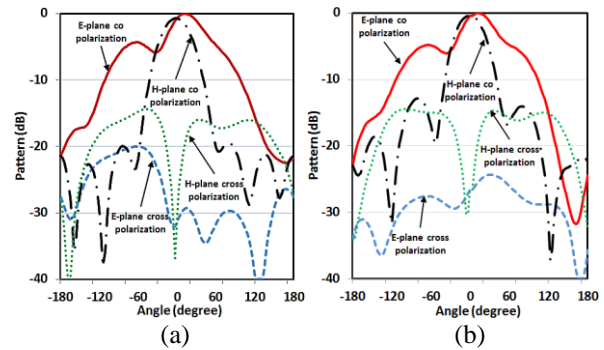


Fig. 7. Simulated co and cross polarizations for radiation patterns at: (a) 2.4 GHz and (b) 2.5 GHz.

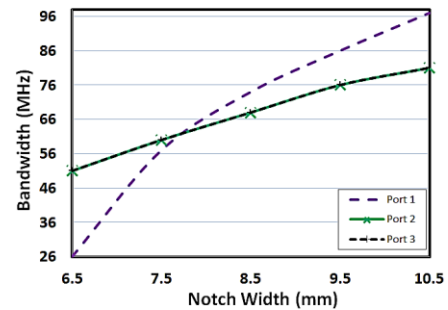


Fig. 8. Bandwidth response as W_{slot} varies [16].

B. ADS circuit model design

The circuit model is designed by substituting the dimensions in Table 2 into (12) – (21) and the parameters found are summarized in Table 3. For optimum output matching, C_{centre} and C_{side} are respectively tuned to 45.5 pF and 52 pF, through gradual decrements of the capacitances with reference to realistic part values.

It is noted that L_{side} appears lower than L_{centre} . This is attributed to the dimension for S_{centre} , which is deliberately elongated as shown in Fig. 6 (a), yielding a longer current path in the centre and thereby causing the higher inductance. This is necessary as the inductance and capacitance of a regular-sized S_{centre} is insufficient

to produce the dual resonance in close proximity. This method forces both frequencies to resonate at 100 MHz apart, without causing additional parasitic which may be deleterious to its performance.

Table 3: Circuit model parameters for proposed antenna

Parameters	Value
$R_{dominant}$	441.0 Ω
$C_{dominant}$	0.4 pF
R_{side}	63.0 Ω
L_{side}	83.0 pH
C_{side}	53.0 pF optimized to 52.0 pF
R_{centre}	63.0 Ω
L_{centre}	87.0 pH
C_{centre}	46.7 pF optimized to 45.5 pF

C. Measurement and simulation

The proposed E-shaped antenna is evaluated base on its 10 dB RL, which is expressed with its reflection coefficients specification (spec) given as:

$$\begin{cases} S_{11} < -10 \text{ dB}, & f = 2.5 \text{ GHz} \\ S_{22}, S_{33} < -10 \text{ dB}, & f = 2.4 \text{ GHz} \end{cases} \quad (22)$$

The fabricated antenna is shown in Fig. 9, while its measured reflection coefficients and simulated reflection coefficients for the ADS Momentum and circuit model designs are plotted in Fig. 10.

The deviation of less than 4 dB between the circuit model design and the actual measurement deems that both results are co-related. It is observed that the notches for all three plots dip about its respective frequency of interest. This ascertains that the ports match remarkably at its designated frequency. It is also evident that the antenna performance complies to the spec with sufficient margins as indicated below the spec line. The plots signify that the circuit model simulated results agree coherently with the ADS Momentum simulated results as well as its measured performance. This justifies the rationale of the postulations in the cavity model.

The minor discrepancies observed between the circuit model and the measured reflection coefficients are conceivably due to the parasitic and coupling losses associated to the measurement setup that are unprecedented in the circuit model. Nevertheless, its theoretical explication is pragmatically sufficient for the analysis of an E-shaped patch design.

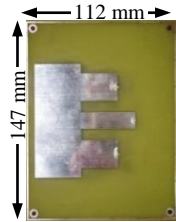


Fig. 9. Fabricated E-shaped antenna board.

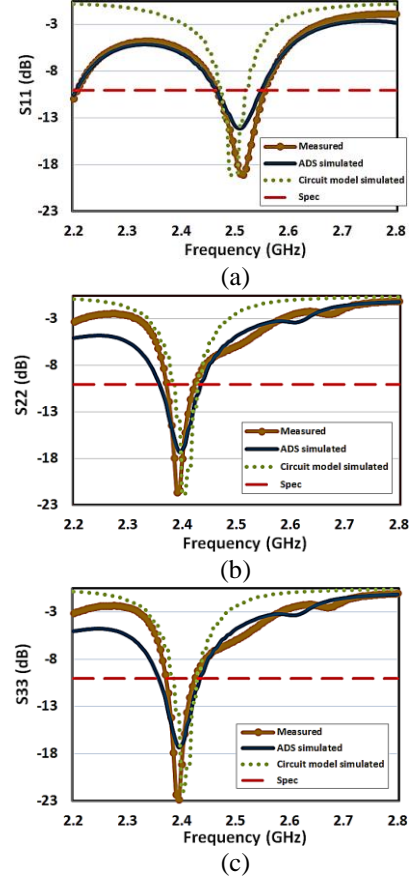


Fig. 10. (a) S_{11} , (b) S_{22} , and (c) S_{33} of the proposed E-shaped antenna as well as its circuit model.

Additionally, by substituting $W_{dominant}$ into W of (11), f_r is found as 2.2 GHz. This result appears close to the desired resonances at 2.4 GHz and 2.5 GHz of the proposed design, and thus signifies the correlation between the theoretical and its actual resonances.

V. CONCLUSION

In overall, the current distribution on the E-shaped antenna visualizes a magnetic wall along the centre of the patch. This in turn implicates its cavity model with two complementary halves. Meanwhile, its circuit model offers an alternative approach in analyzing the dual resonance effect. Rather than involving complex computations and refined meshes, this model characterizes the matching point of the antenna in a much simplistic manner. The results are almost instantaneous compared to the ADS Momentum simulation. In the generality of antenna practice, this analytical approach is believed to play an influential role in future antenna research of arbitrary shapes.

REFERENCES

- [1] J. Miranda, J. Cabral, B. Ravelo, S. Wagner, C. F. Pedersen, M. Memon, and M. Mathiasen,

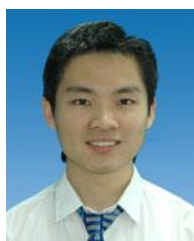
- “Radiated EMC immunity investigation of common recognition identification platform for medical applications,” *Eur. Phys. J. Appl. Phys.*, vol. 69, no. 1(11002), pp. 1-8, Jan. 2015.
- [2] F. Yang, X. Zhang, X. Ye, and Y. Rahmat-Samii, “Wide-band E-shaped patch antennas for wireless communications,” *IEEE Trans. Antennas Propag.*, vol. 49, no. 7, pp. 1094-1100, July 2001.
- [3] M. B. Kadu, R. P. Labade, and A. B. Nangaonkar, “Analysis and designing of E-shape microstrip patch antenna for MIMO application,” *Int. J. of Eng. and Innovative Technol.*, vol. 1, no. 2, pp. 67-69, Feb. 2012.
- [4] B. K. Ang and B. K. Chung, “A wideband E-shaped microstrip patch antenna for 5-6 GHz wireless communications,” *Prog. Electromagn. Res.*, vol. 75, pp. 397-407, 2007.
- [5] V. K. Pandey and B. R. Vishvakarma, “Analysis of an E-shaped patch antenna,” *Microw. Opt. Technol. Lett.*, vol. 49, no. 1, pp. 4-7, Jan. 2007.
- [6] Z. Manzoor and G. Moradi, “Optimization of impedance bandwidth of a stacked microstrip patch antenna with the shape of parasitic patch’s slots,” *Appl. Comput. Electromagn. Society (ACES) J.*, vol. 30, no. 9, pp. 1014-1018, Sep. 2015
- [7] Y. Ge, K. P. Esselle, and T. S. Bird, “E-shaped patch antennas for high-speed wireless networks,” *IEEE Trans. Antennas Propag.*, vol. AP-52, no. 12, pp. 3213-3219, Jan. 2005.
- [8] A. A. Deshmukh and G. Kumar, “Compact E- and S-shaped microstrip antennas,” *Electron. Lett.*, vol. 3B, pp. 389-392, July 2005.
- [9] P. K. Singhal and P. Moghe, “Design of a single layer E-shaped microstrip patch antenna,” *Asia Pac. Microw. Conf.*, Suzhou, China, Dec. 2005.
- [10] Y. Ge, K. P. Esselle, and T. S. Bird, “Broadband E-shaped patch antennas for 5-6 GHz wireless computer networks,” *IEEE Antennas Propag. Society Int. Symp.*, pp. 942-945, June 2003.
- [11] N. Ojaroudi, S. Amiri, F. Geran, and M. Ojaroudi, “Band-notched small monopole antenna using triple E-shaped structures for UWB systems,” *Appl. Comput. Electromagn. Society (ACES) J.*, vol. 27, no. 12, pp. 1022-1028, Dec. 2012.
- [12] B. Ravelo, “Synthesis of n-way active topology for wide-band RF/microwave applications,” *Int. J. Electron.*, vol. 99, no. 5, pp. 597-608, May 2012.
- [13] K. L. Wong and W. H. Hsu, “A broad-band rectangular patch antenna with a pair of wide slits,” *IEEE Trans. Antennas Propag.*, vol. 49, no. 9, pp. 1345-1347, Sep. 2001.
- [14] Y. T. Lo, D. Solomon, and W. F. Richards, “Theory and experiment on microstrip antennas,” *IEEE Trans. Antennas Propag.*, vol. 27, no. 2, pp. 137-145, Mar. 1979.
- [15] C. A. Balanis, *Antenna Theory, Analysis and Design*. John Wiley & Sons, 2005.
- [16] K. H. Yeap, W. Ismail, S. L. Yap, and K. H. Yeap, “Parametric study for E-shaped microstrip patch antenna,” *Malaysian J. of Science*, vol. 35, no. 2, pp. 284-318, Dec. 2016.
- [17] K. F. Lee and W. Chen, *Advances in Microstrip and Printed Antennas*. Wiley, 1997.
- [18] S. K. Patel and Y. P. Kosta, “E-shape microstrip patch antenna design for GPS application,” *Int. Conf. Current Trends Technol.*, Dec. 2011.
- [19] C. Yildiz and K. Guney, “Simple model for the input impedance of rectangular microstrip antenna,” *J. of Eng. Sciences*, vol. 4, no. 3, pp. 733-738, 1998.
- [20] Technical Report 00929 Physical Science Laboratory, Theoretical Investigation of the Microstrip Antenna, New Mexico State University, 1979.
- [21] K. Guney, “Radiation quality factor and resonant resistance of rectangular microstrip antenna,” *Microw. Opt. Technol. Lett.*, vol. 7, no. 9, pp. 427-430, June 1994.



Kim Huat Yeap received his B.Eng. (Hons.) from Universiti Tenaga Nasional in 2004 and M.Sc. from Universiti Sains Malaysia in 2012. He is currently pursuing his Ph.D. in Universiti Sains Malaysia. His research interest focuses in the areas of antennas and mixers.



Widad Ismail received her B.Eng. (Hons.) from University of Huddersfield in 1999 and Ph.D. from University of Birmingham in 2004. She is currently a Professor in School of Electrical and Electronic Engineering, Universiti Sains Malaysia. Her research interest focuses in the area of antennas, mixers, and Radio Frequency identification systems.



Kim Ho Yeap received his B.Eng. (Hons.) from Universiti Teknologi Petronas in 2004, M.Sc. from Universiti Kebangsaan Malaysia in 2005, and Ph.D. from Universiti Tunku Abdul Rahman in 2011. He is currently an Associate Professor in Faculty of Engineering and Green Technology, Universiti Tunku Abdul Rahman. His research interest includes microelectronics devices, waveguides, and radio telescopes.